Line-of-sight Millimeter-wave Communications using Orbital Angular Momentum Multiplexing Combined with Conventional Spatial Multiplexing

Yongxiong Ren, Long Li, Guodong Xie, Yan Yan, Yinwen Cao, Hao Huang, Nisar Ahemd, Zhe Zhao, Peicheng Liao, Chongfu Zhang, Martin P. J. Lavery, Moshe Tur, *Fellow, IEEE,* Giuseppe Caire, *Fellow, IEEE,* Andreas F. Molisch, *Fellow, IEEE,* and Alan E. Willner, *Fellow, IEEE*

***Abstract*—Line-of-sight wireless communications can benefit from the simultaneous transmission of multiple independent data streams through the same medium in order to increase system capacity. A common approach is to use conventional spatial multiplexing with spatially separated transmitter/receiver antennae, for which inter-channel crosstalk is reduced by employing multiple-input-multiple-output (MIMO) signal processing at the receivers. Another fairly recent approach to transmitting multiple data streams is to use orbital-angular-momentum (OAM) multiplexing, which employs the orthogonality among OAM beams to minimize inter-channel crosstalk and enable efficient (de)multiplexing. In this paper, we explore the potential of combining both of these multiplexing techniques such that they complement each other and enhance system performance. We demonstrate a 16-Gbit/s millimeter-wave communication link using OAM multiplexing over conventional spatial multiplexing. Specifically, we implement a spatial multiplexing system with a 2×2 antenna aperture architecture, in which each transmitter aperture contains two multiplexed 4-Gbit s-1 data-carrying OAM beams. A MIMO-based signal processing is used at the receiver to mitigate interferences among the channels. Our experimental results show performance improvements for all channels after MIMO processing, with uncoded bit-error rates of each channel below 3.8×10^{-3}. Our results also indicate that OAM multiplexing and conventional spatial multiplexing combined with MIMO processing can be compatible with and complement each other.**

***Index Terms*—mm-wave communications, orbital angular momentum, spatial multiplexing.**

Manuscript received April XX, 2016. This work is supported by the Intel Labs University Research Office

Y. Ren, L. Li, G. Xie, Y. Yan, Y. Cao, H. Huang, N. Ahmed, Z. Zhao, P. Liao, G. Caire, A. F. Molisch, and A. E. Willner are with the Department of Electrical Engineering, University of Southern California, Los Angeles, CA 90089 USA (e-mail: yongxior@usc.edu).

C. Zhang is with School of Communication and Information Engineering, University of Electronic Science and Technology of China, Chengdu 611731, China.

M. P. Lavery is with School of Physics and Astronomy, University of Glasgow, Glasgow, G12 8QQ, UK.

M. Tur is with School of Electrical Engineering, Tel Aviv University, Ramat Aviv 69978, Israel.

I. Introduction

Line-of-sight (LOS) wireless communications with fixed transmitter and receiver locations is of increasing importance for its potential in many applications, including cellular back-haul and interconnections within a data center [1-4]. Given the rapid growth of bandwidth demand for these applications, there is great interest in utilizing advanced multiplexing of multiple data streams to dramatically increase the data capacity and spectral efficiency of an LOS communication system [5]. An important approach is to use spatial multiplexing with multiple antenna elements at transmitter/receiver combined with multiple-input multiple-output (MIMO) signal processing [6-9]. With proper antenna spacing, this provides enormous capacity gains relative to single antenna systems [4, 9-14].

Another potential approach for simultaneously transmitting multiple data streams is to use a set of orthogonal electromagnetic (EM) waves [15, 16]. Such a system transmits multiple coaxially propagating, spatially-overlapping waves each carrying an independent data stream through a single aperture pair. Therefore, the total capacity and spectral efficiency of the communication system can be increased by a factor equal to the number of transmitted orthogonal modes. An orthogonal spatial modal basis set that has recently received increasing interest is orbital angular momentum (OAM) [17-20]. An EM wave with a helical transverse phase of the form $\exp(i\ell\emptyset)$ carries an OAM corresponding to $\ell\hbar$, where $\emptyset$ is the azimuthal angle, ℓ is an unbounded integer (the OAM state number), and $\hbar$ is the reduced Planck's constant [17]. Importantly, OAM modes with different ℓ values are mutually orthogonal, allowing them to be efficiently (de)multiplexed and utilize the same single transmitter/receiver aperture pair with low inter-channel crosstalk [16, 21].

OAM modes have been used to demonstrate high-capacity communications in the optical domain as well as at radio frequencies (RF) [15, 21-23]. Recently, a 32 Gbit/s millimeter-wave (mm-wave) data link using OAM multiplexing combined with polarization multiplexing over a

single aperture pair has been reported, in which all OAM beams were multiplexed together and propagated along the same spatial axis [24]. This single-aperture-pair approach employs the orthogonality of OAM beams to minimize inter-channel crosstalk and enable recovery of different data streams, thereby avoiding the use of MIMO processing [6, 25]. This is different from conventional spatial multiplexing, for which each data-carrying beam is received by multiple spatially separated receivers and MIMO-based signal processing is critical for reducing the crosstalk among channels and thus allows data recovery [26-29].

However, MIMO-based signal processing becomes more onerous for conventional spatial multiplexing systems as the number of antenna elements increases, especially at high data rates (Gbit/s) [25, 29]. Moreover, for OAM multiplexing systems, the detection of high-order OAM modes presents a challenge for the receiver because OAM beams with larger ℓ values diverge more during propagation [15, 20]. Therefore, the achievable number of data channels for each type of multiplexing technique might be limited, and achieving a larger number of channels by using any one approach might be significantly more difficult [8, 24, 25]. There might exist the possibility of partially exploiting the advantages of each multiplexing technique and simultaneously utilizing both techniques to increase system performance [30-32]. If each antenna aperture in a conventional spatial multiplexing system can transmit multiple independent information-carrying OAM beams, the total number of channels accommodated could be further increased, thereby increasing system transmission capacity. Furthermore, the complexity of implementing MIMO processing in such a system could be potentially reduced by exploiting the orthogonality of OAM beams. Note that these two multiplexing techniques employ the same degrees of freedom for multiplexing, which means that the full benefits of OAM and spatial multiplexing cannot be reaped simultaneously.

In this paper, we experimentally demonstrate a 16-Gbit/s mm-wave communication link using OAM multiplexing combined with conventional spatial multiplexing. A spatial multiplexing system with a 2×2 antenna aperture architecture, each transmitter aperture containing multiplexed OAM beams with ℓ =+1 and +3, is implemented. Each of the four OAM channels carries a 1-Gbaud 16 quadrature amplitude modulation (16-QAM) signal at a carrier frequency of 28 GHz, thereby achieving a capacity of 16 Gbit/s (1 Gbaud × 4 bit per symbol × 4 OAM channels) [30]. After propagating through 1.8 meters, the OAM beams from one transmitter aperture spatially overlap those from the other apertures at the receiver aperture planes, resulting in crosstalk among non-coaxial OAM channels. A 4×4 MIMO signal processing is used to mitigate the channel interferences. Our experimental results show that the performance of each channel improves after MIMO processing, with uncoded bit-error rates below 3.8×10^{-3}. This indicates that OAM multiplexing and conventional spatial multiplexing combined with MIMO processing can be compatible with and complement each other, thereby providing potential to enhance system performance. Under certain design trade-offs and limitations, this indicates that OAM multiplexing and conventional spatial multiplexing could be simultaneously utilized to distribute the spatial degrees of freedom of an LOS system, thereby providing system design flexibility and potentially enhancing system performance; as will be explained later in the paper, we emphasize that these two multiplexing techniques are not independent, but involve some system trade-offs when utilized together, and cannot be simply multiplied together.

II. Concept and Experimental Setup

The concept of a high-capacity LOS wireless link using OAM multiplexing combined with MIMO-based spatial multiplexing architecture is depicted in Figure 1. This system might be suitable for application scenarios that require short range, high speed wireless information transmission. The system consists of N transmitter/receiver aperture pairs that are arranged in a uniform linear structure. Each of the transmitter apertures T_i $(i = 1,2,\dots,N)$ transmits M multiplexed OAM beams, resulting in a total number of NM OAM data channels. The N receiver apertures R_i $(i = 1,2,\dots,N)$ are used to capture the fields transmitted from the N transmitter apertures. Because of divergence along the propagation distance, the OAM beams

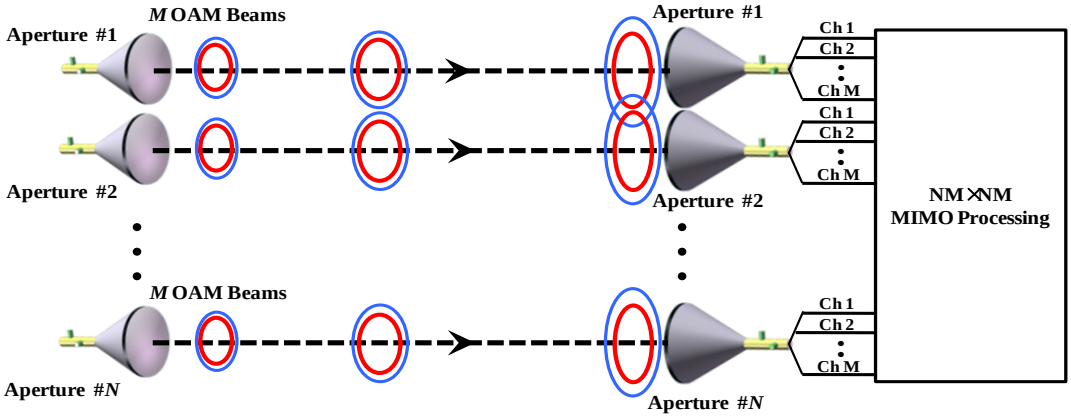

Figure 1. Concept of a line-of-sight mm-wave communications link employing OAM multiplexing over conventional spatial multiplexing. The system consists of N transmitter/receiver apertures, with each transmitter aperture containing M OAM modes. This technique could have potential applications in scenarios, such as data centers and back-haul connections that require high-capacity data transmission.

from each transmitter aperture may spatially overlap at the receiver. The received signal vector at receiver aperture R_i, $y_i = (y_{i,1}, y_{i,2}, \dots, y_{i,M})^T$ can be expressed as

$$y_i = \sum_{j=1}^{N} h_{i,j} x_j + n_i, \quad (1)$$

where $y_{i,m}$ $(m = 1,2, \dots M)$ is the received signal of the m-th OAM channel in the i-th receiver aperture, $x_j = (x_{j,1}, x_{j,2}, \dots, x_{j,M})^T$ is the transmitted signal vector for M OAM channels from transmitter aperture T_j, $h_{i,j}$ is an $M \times M$ matrix depicting the transfer function (possibly frequency-dependent) between OAM channels from aperture T_j to R_i, and n_i is the noise vector for R_i. Note that ideally $h_{i,i}$ is a diagonal matrix resulting from the orthogonality between M transmitted co-axial OAM modes and its diagonal entries are not necessarily similar due to different diffraction among OAM channels. Therefore, the channel transfer matrix between NM OAM channels H can be written as

$$H = \begin{bmatrix} h_{1,1} & h_{1,2} & \cdots & h_{1,N} \\ h_{2,1} & h_{2,2} & \cdots & h_{2,N} \\ \vdots & \vdots & \ddots & \vdots \\ h_{N,1} & h_{N,2} & \cdots & h_{N,N} \end{bmatrix}_{NM \times NM}, \quad (2)$$

from which the total crosstalk of each OAM channel can be estimated. H is determined by the overlaps between OAM beams from different transmitter apertures, which are directly related to the propagation distance, antenna design and transmitter/receiver aperture spacing.

We demonstrate below a proof-of-concept experiment using a 2×2 aperture architecture, each transmitter aperture containing two multiplexed mm-wave OAM beams at a carrier frequency of 28 GHz ($N = M = 2$). Figures 2 and 3 show the schematic and photos of experimental setup, respectively. At the transmitter, a 28 GHz continuous-wave (CW) signal is first

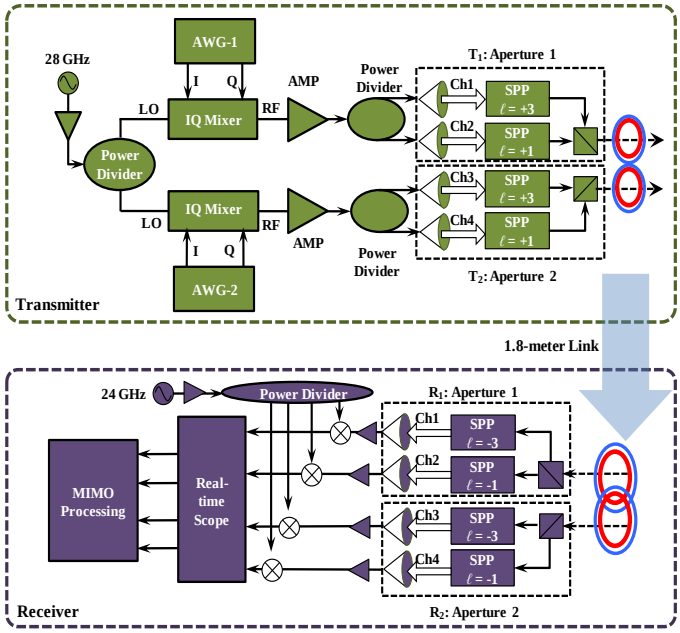

Figure 2. Experimental setup of a 16-Gbit/s mm-wave link using MIMO processing of 2 OAM beams, each on 2 transmitter/receiver antenna apertures. AMP: amplifier, AWG: arbitrary waveform generator, Ch: channel, T_i: Transmitter aperture i; SPP: spiral phase plate; R_i: Receiver Aperture i.

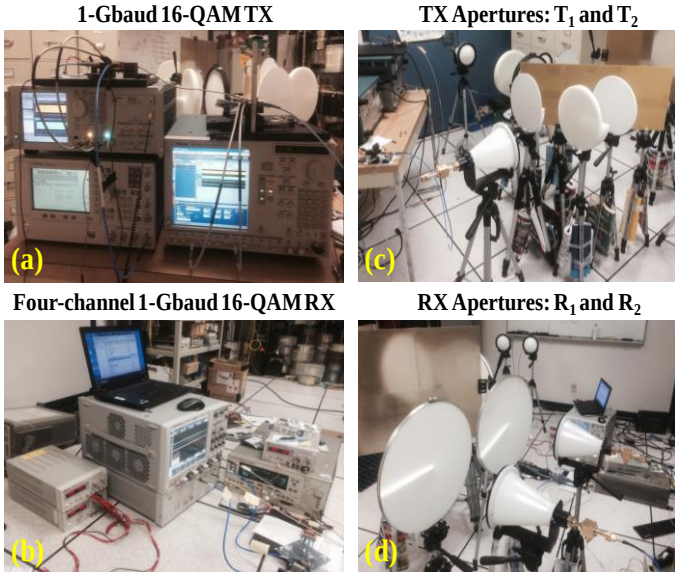

Figure 3. Photos of the experimental setup. (a) 1-Gbaud 16-QAM signal generation for all four channels. (b) Simultaneous detection of four 1-Gbaud 16-QAM channels. (c) Generation and multiplexing of OAM beams at T_1 and T_2. (d) Demultiplexing and detection of OAM beams at R_1 and R_2. TX: Transmitter. RX: Receiver.

amplified and then split into two paths, which serve as local oscillator signals for the two I/Q mixers. Two arbitrary waveform generators (Tektronix AWG 7102 and AWG 70002A) are used to generate two independent pairs of I and Q waveforms of 1-Gbaud four-level amplitude-modulation signals and are connected to the intermediate frequency ports of the two I/Q mixers, creating two independent 1-Gbaud 16-QAM data streams at a carrier frequency of 28 GHz. No pulse shaping or pre-filtering technique is used and the bandwidth of the signals is ~1 GHz. Each of the two 16-QAM data streams is amplified and split into two paths, which are relatively delayed using cables of different lengths, and fed to two collimated lensed horn antennae with diameters of 15 cm. Due to time delays, the four 16-QAM data streams are mutually decorrelated and can be considered four independent channels. We believe this will not affect the power transfer and crosstalk among channels. The amplitude of each generated I/Q waveform is adjusted to equalize the transmitted signal power for all four channels. The output of each antenna is converted to an OAM beam (either $\ell = +1$ or $\ell = +3$) by passing through a spiral phase plate (SPP) with a specific ℓ value [33, 34]. The SPPs that are used to generate the OAM beams are manufactured through the computer numerical control milling of a solid block of high-density polyethylene, which has a refractive index of 1.52 at 28 GHz. The SPPs have circular apertures with diameters of 30 cm. The size of the SPP is larger than that of the lensed-horn antenna in order to limit possible effects that may arise from a truncated aperture.

The two generated OAM beams $\ell = +1$ and $\ell = +3$ in each transmitter aperture are spatially combined by a mm-wave beam splitter. This beam splitter is similar in form to the polka-dot beam splitter used in the optical regime and is fabricated by patterning a standard printed circuit board (PCB) with a designed structure [24]. In our experiment, two lensed

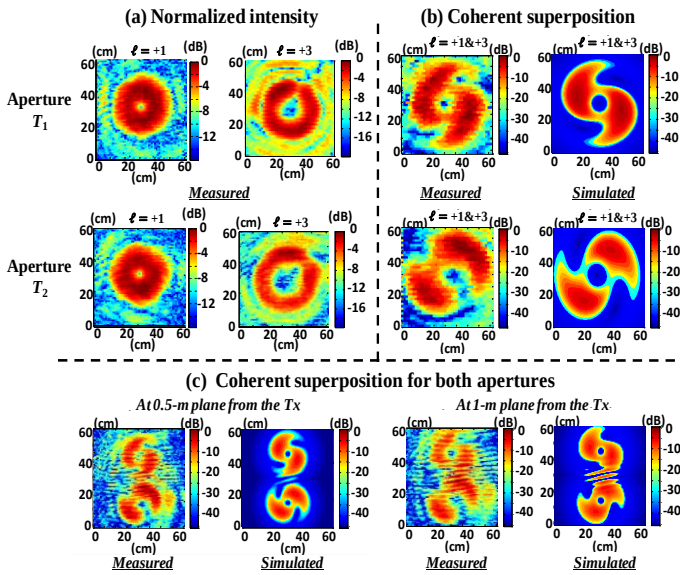

Figure 4. Normalized intensity and superpositions of mm-wave OAM beams. (a) Normalized measured intensity of mm-wave OAM beams ℓ =+1 and ℓ =+3 in transmitter apertures T_1 or T_2. (b) Normalised measured and simulated superpositions of OAM beams ℓ =+1 and ℓ =+3 at T_1 or T_2 plane. (c) Normalized measured and simulated superpositions of all four OAM beams at 0.5-metres or 1-meters plane from the transmitter. Tx: transmitter.

horn antennae along with two SPPs and a mm-wave beam splitter are grouped together to implement a transmitter aperture T_1 or T_2, as depicted in Figure 2. Ideally, it would be desirable to have an integrated device that can simultaneously generate and multiplex multiple independent OAM beams [35-37]. The resulting multiplexed OAM beams from T_1 and T_2, which are separated by 32 cm, are respectively transmitted towards the receiver apertures R_1 and R_2 located at a distance of 1.8 meters.

Figure 4 shows the measured normalized intensity of the generated OAM beams, and their normalized spatial coherent superpositions. These intensity profiles are captured via a probe antenna with a small aperture diameter of 0.7 cm, whose output is recorded by an RF spectrum analyzer. The probe antenna is attached to a two-dimensional (X-Y) linear translation stage with a scanning resolution of 1 cm and a transversal coverage area of 60×60 cm. The ring-shaped intensity profile of the generated mm-wave OAM beams, clearly depicted in Figure 3a, confirms that an OAM beam with $\ell = +3$ diverges faster than that with $\ell = +1$. The state number of the OAM beams (ℓ =+1 and ℓ =+3) can be deduced from the number of rotating arms in Figure 3b, which shows the measured intensity distribution of coherent superposition of OAM beams ℓ =+1 and ℓ =+3 at T_1 or T_2 planes. Also, the coherent superpositions of all four OAM beams measured at 0.5-metres or 1-meters plane from the transmitter, as shown in Figure 3c, illustrate that the overlaps between OAM beams from apertures T_1 and T_2 increase with the transmission distance. These measured OAM beams superpositions are corroborated by the corresponding simulation results.

Similar to the transmitter architecture, a pair of lensed horn antennae along with SPPs, and a mm-wave beam splitter are grouped together to implement the receiver aperture R_1 or R_2. Each of the SPPs in the receiver apertures has a conjugate phase relationship with that of the corresponding SPP in the transmitter apertures, allowing the OAM beam to be converted back to a planar-phased beam. This beam has a bright high-intensity spot at the centre, which is separable from the other co-axial OAM beam with a 'doughnut' intensity profile through spatial filtering. This beam can be efficiently collected by a lensed horn antenna that is matched to the Gaussian beams ($\ell = 0$). For example, in order to obtain the data stream carried on OAM $\ell = +1$ from T_1, an inverse SPP with the opposite thickness profile ($\ell = -1$) is employed. Consequently, the helical phase of the $\ell = +1$ OAM beam is removed, and the other co-axial OAM beam $\ell = +3$, while also transformed by the SPP ($\ell = +3 \rightarrow \ell = +2$), maintains its ring-shaped profile and helical phase; therefore, negligible signal can be coupled into the Gaussian-matched antenna due to the mode mismatch. However, due to the divergence of the transmitted OAM beams and a small separation of 32 cm between the two receiver apertures, the OAM beams from the two transmitter apertures spatially overlap at the receiver aperture planes. Therefore, part of the non-axial OAM beams from the neighboring transmitter aperture would also be coupled into the receiver antenna, resulting in channel crosstalk.

III. Crosstalk Measurements

We characterize the power leakage and crosstalk between all OAM channels. To simplify these measurements, we measure the power leakage at 28 GHz for each channel by transmitting a 28 GHz CW signal rather than 1-Gbaud 16-QAM modulated signals. This is an approximation, since our RF-modulated signal spectrally lies within 28±1GHz and our SPPs and beam splitters are frequency-dependent. The power leakage is measured in the following way: We first transmit a 28 GHz CW signal over OAM ℓ=+1 in T_1 while all the other channels (OAM ℓ=+3 in T_1 and OAM ℓ=+1/ℓ=+3 in T_2) are off. Then we record the received power for each received antenna (OAM

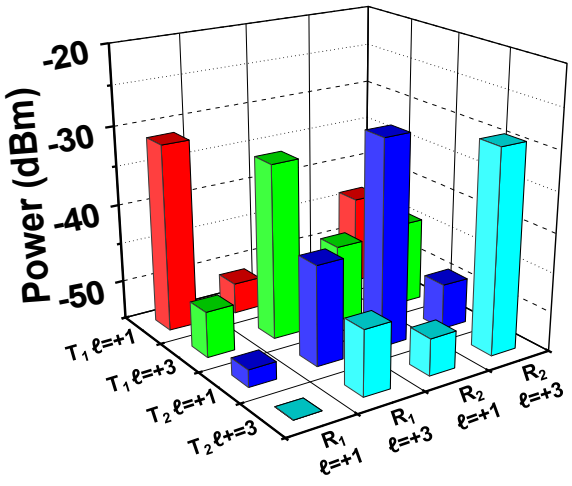

Figure 5. Power transfer matrix of all four OAM channels. Received power measured for ℓ=+1 and ℓ=+3 in R_1 and R_2 when only transmitting channel ℓ=+1 or ℓ=+3 at T_1 or T_2, respectively. The data is measured by transmitting a 28 GHz CW signal.

ℓ=+1 and ℓ=+3 for both R_1 and R_2) using an RF spectrum analyzer. The above measurements are repeated for all transmitted OAM channels until a full 4×4 power transfer matrix is obtained, as shown in Figure 5. We note that the power transfer matrix can be directly calculated from a known channel matrix $\boldsymbol{H}$. We see that the power leakages of channel ℓ=+3 to the two non-coaxial channels are larger than those of channel ℓ=+1, since OAM beam ℓ=+3 diverges faster, resulting in a larger overlapping area at the receiver plane. In addition, there exists a small amount of power leakage between the coaxial channels ℓ=+1 and ℓ=+3, due to the imperfections of OAM generation, multiplexing, and setup misalignment. In an ideal case, the two coaxial channels should be perfectly isolated by the orthogonality of coaxial propagating OAM beams.

The total crosstalk of a specific channel can be calculated from the 4×4 power transfer matrix by adding the received power from all other channels divided by the received power of this channel. Since the transmitted signal is wideband, the actual crosstalk values are expected to be slightly larger than the measured values. We observe that the crosstalk between coaxial OAM channels are all below -18 dB and major power transfers occur between non-coaxial channels. The total crosstalk values for channels ℓ=+1/ℓ=+3 of R_1 and R_2 are -15.7 dB, -8.8 dB, -14.8 dB, -11.1 dB, respectively. We also see that ℓ=+3 experiences larger crosstalk than ℓ=+1 for both the receiver apertures, which is determined by the overlapping between all OAM beams at the receiver plane in a particular system. Also, the crosstalk values of ℓ=+1/ℓ=+3 in the two receiver apertures are slightly different. However, in principle, the crosstalk of channels with the same OAM state number in different receiver apertures should be identical, if the transmitter/receiver aperture pairs are built symmetrically.

IV. Multiple-Input Multiple-Output Based Signal Processing Algorithm

MIMO post-processing has long been used in conventional spatial multiplexing (for a non-diagonal channel matrix $\boldsymbol{H}$) to reduce channel interferences and thus recover the transmitted data streams. A variety of implementation approaches for MIMO processing have been proposed [5, 8, 25, 29, 38], including joint maximum likelihood sequence estimation of the data symbols in different streams, minimum mean-square error detection combined with serial interference cancellation across the antennae (also known as BLAST), zero forcing detection, and pilot-aided channel equalization.

In our experiment, we use multi-modulus algorithm (MMA)-based equalization [39, 40] for MIMO processing. 4×4 MMA-MIMO digital signal processing (DSP) [41] is implemented to reduce the interference among channels and recover the four data streams. To simultaneously detect all four channels, the signal received from each receiver antenna is amplified and down-converted to a 4 GHz carrier frequency by mixing with a 24 GHz CW signal. The four signals after down-conversion are sampled by a four-channel 80 GSample/s real-time scope with a bandwidth of 16 GHz on each channel and recorded for offline DSP. The procedures of the DSP are depicted in Figure 6a. Each of four sequences (from OAM channel ℓ=+1 and ℓ=+3 of R_1 and R_2) is converted to the frequency domain and then band-pass filtered, followed by a 4-GHz frequency shift to baseband. The signals are then converted back to time domain and down-sampled to 2 samples per symbol. The MIMO adaptive equalization algorithm utilizes a linear equalizer for each channel [39-41]. For a 4×4 MIMO equalization, the equalizer includes 16 adaptive finite-impulse-response (FIR) filters, each with a tap number of K. We emphasize that the FIR filters can help cancel the temporal misalignment between the four received signals and temporal inter-symbol interference (ISI) of each channel

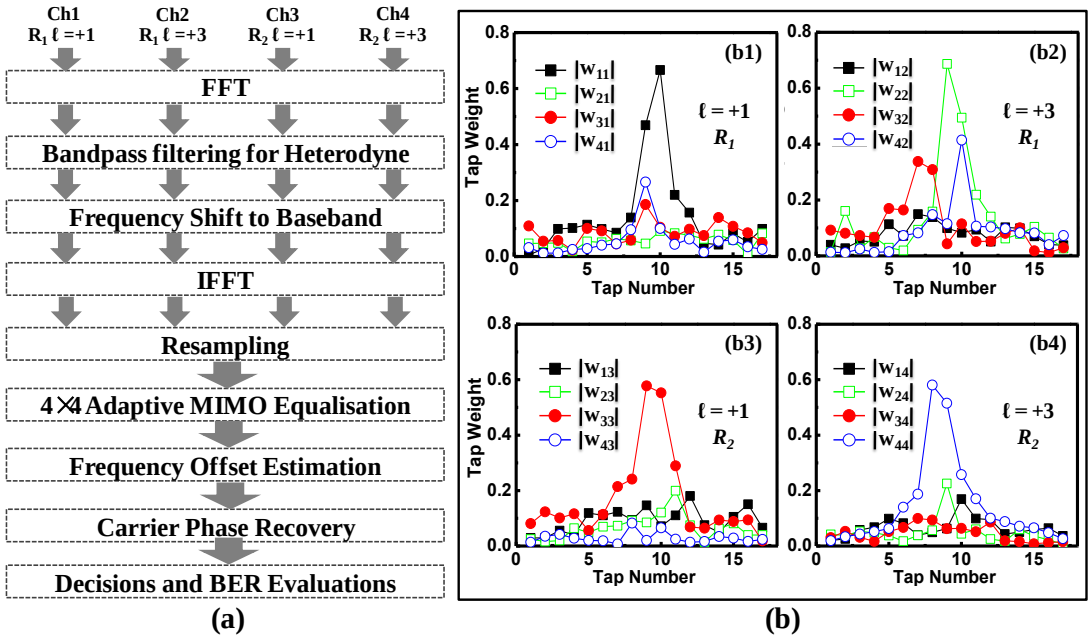

Figure 6. MIMO-based digital signal processing. (a) The procedures of off-line digital signal processing. (b) Convergent tap weight (FIR filter coefficients) of the equalizer using multi-modulus algorithm (MMA). (b1-b4) The absolute value of complex taps weights of the four FIR filters to equalize Ch1 (ℓ=+1 in R_1), Ch2 (ℓ=+3 in R_1), Ch3 (ℓ=+3 in R_2), and Ch4 (ℓ=+3 in R_2), respectively.

induced by non-ideal filtering and sampling. The output of the equalizer corresponding to each channel can be expressed as:

$$y_j = \sum_{i=1}^{4} \boldsymbol{w_{ij}} * \boldsymbol{x_i}, j = 1, 2, 3, 4 \qquad (3)$$

where w_{ij} (i =1, 2, 3, 4) is the coefficient vector of the FIR filter with a vector length of K (tap number), x_i is the input signal vector of the i-th channel. $w_{ij} * x_i$ represents the inner product operation between two vectors, and y_j is the output of the FIR filter. All the FIR coefficients are initialized as zero with only the centre weight being 1, and then updated until the coefficients converge based on MMA [39, 40]:

$$\boldsymbol{w_{ij}}(k+1) = \boldsymbol{w_{ij}}(k+1) + u \cdot e_i \cdot y_i \cdot \boldsymbol{x_i}^* \qquad (4)$$

where u is the step size, $e_i = P_{ref} - |y_i|^2$ is the error signal of the adaptive estimation, and P_{ref} is the normalized reference power of the 16-QAM signal. The main idea of MMA-MIMO algorithm is to update filter weights such that each channel output can have clear discrete amplitudes [42]. For the 16-QAM modulation format used here, signals with 3 clear discrete amplitudes are preferred as the output. The tap number K in each FIR filter is set to be 17, which is enough to cover the differential time delays among each data sequence and mitigate temporal ISI effects. Figure 6b shows the converged tap weights of the 16 FIR filters after 10,000 iterations. As an example, Figure 6(b1) illustrates the tap weights of four FIR filters (w_{11}, w_{21}, w_{31}, and w_{41}) that are used to generate the equalized output for channel ℓ=+1 of R_1. We see that for the equalization of a specific channel, the tap weights of the FIR filters corresponding to its coaxial OAM channel are low (less than 0.1, generally), due to the negligible interference between them. The obtained FIR filter coefficients are used to estimate the channel transfer matrix and equalize the crosstalk among four OAM channels based on Eq. 3. After equalization, the frequency offset estimation and the carrier phase recovery are applied to recover signal constellations, and the bit-error rates (BERs) are evaluated for all channels.

In a general case, given that channel matrix $\boldsymbol{H}$ has N diagonal $M \times M$ sub-matrices along its main diagonal line (N is the number of transmitter/receiver aperture pairs and M is the number of OAM beams in each transmitter aperture), a smaller number of other channels needs to be considered when equalizing a specific channel in MIMO processing, indicating a lower computation complexity. For the FIR-MMA equalization approach used in our experiment, the post-processing complexity for an $NM \times NM$ channel matrix $\boldsymbol{H}$ is proportional to $NM \times (N-1)M \times K$ [39-41]. This is reduced by half when $N = 2$, compared to a regular $\boldsymbol{H}$ with its processing complexity proportional to $NM \times NM \times K$.

V. BER MEASUREMENTS

Figure 7a shows the BER measurements of 1-Gbaud 16-QAM signals for channels ℓ=+1 and ℓ=+3 when only one transmitter/receiver aperture pair is on. In this case, there is no mutual crosstalk from channels of the other transmitter/receiver pair. The theoretical BER curve of a 16-QAM signal is also plotted as a benchmark. The 16-QAM constellations and error

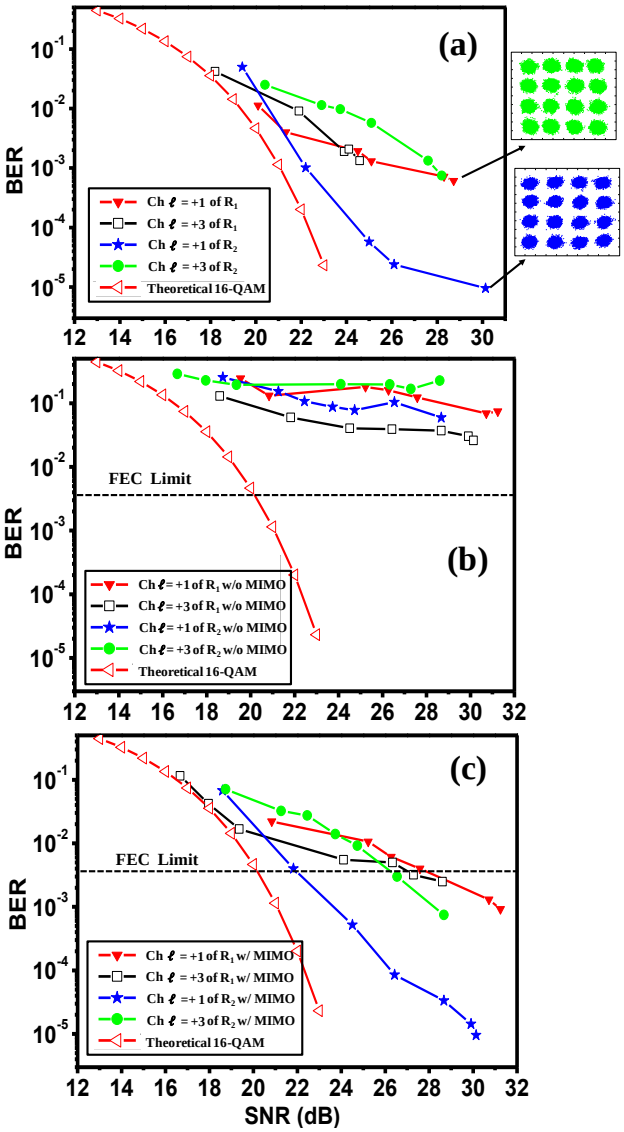

Figure 7. BER measurements of 1-Gbaud 16-QAM signal for channels ℓ=+1 and ℓ=+3 for R_1 (when T_2 is off) and R_2 (when T_1 is off). Measured BERs as a function of received SNR for all four OAM channels (ℓ=+1 and ℓ=+3 in both R_1 and R_2) (b) without MIMO processing and (c) with MIMO processing.

vector magnitudes (EVMs) [43] of the received 1-Gbaud 16-QAM signals with a certain signal-to-noise ratio (SNR) for channel ℓ=+1 in R_1 (SNR = 28.7 dB) and R_2 (SNR = 31.3 dB) are also presented. It is clear that without interference from other apertures, each channel can achieve a raw BER of 3.8×10^{-3}, which is a level that allows to achieve extremely low block error rates through the application of efficient forward error correction codes [44]. We observe that channel ℓ=+1 in R_2 with a higher crosstalk from its coaxial channel ℓ=+3 has a lower power penalty than that in R_1, as expected.

We measure the BERs for all four channels when both T_1 and T_2 are turned on. Here all OAM channels experience crosstalk from both their coaxial and non-coaxial channels. Figure 7(b) shows the measured BERs of all 4 OAM channels without MIMO processing. We see that the BER curves for all four channels exhibit the "error floor" phenomenon due to the strong crosstalk from other channels. We also see that with a SNR

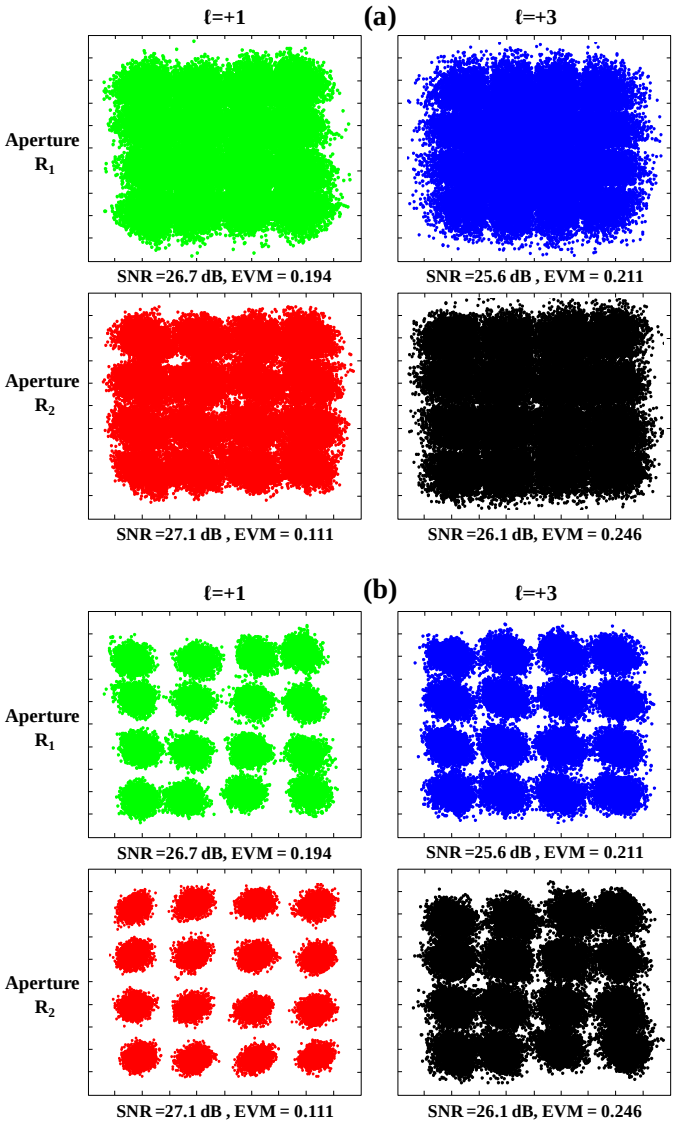

Figure 8. Constellations. The received 1-Gbaud 16-QAM signal constellations for all four OAM channels (ℓ=+1 and ℓ=+3 in both R_1 and R_2) at one acquisition by the real-time scope (a) without MIMO processing and (b) with MIMO processing. The SNR and the EVM for each constellation are also given.

smaller than 30 dB, BERs for all the channels are above 3.8×10^{-3}. Figure 7(c) depicts the BER curves for all four channels under the same conditions using MIMO equalization processing. We observe that the BERs decrease dramatically and can reach below 3.8×10^{-3} for all four channels after MIMO processing. The received constellations of 1-Gbaud 16-QAM signal for OAM channels ℓ=+1 in both R_1 and R_2 are also shown in Figure 8 to further illustrate this improvement. The SNR and the EVM for each constellation are also given and we see that the constellations of channels ℓ=+1 in both apertures exhibit better quality after MIMO processing. We note that the transmission distance in our experiment is 1.8 meters and expanding the link distance depends on several factors, including the receiver aperture size and the OAM beam divergence. For increased distances, less power will be received by a fixed receiver aperture due to the divergence of the OAM beam.

VI. Discussion

From a theoretical perspective, OAM multiplexing can be considered as another form of spatial multiplexing [15, 35, 45-47]. Conventional spatial multiplexing employs multiple spatially separated transmitter and receiver aperture pairs for the transmission of multiple data streams that are recovered through the use of MIMO processing. Alternatively, OAM-based spatial multiplexing transmits multiplexed OAM beams through a single aperture pair, employing OAM beam orthogonality to minimize inter-channel crosstalk and achieve efficient demultiplexing, thus reducing the need for further MIMO processing to mitigate channel interferences.

In our multiplexing system with N transmitter/receiver aperture pairs, in which each transmitter aperture contains M multiplexed OAM channels, a total number of NM data channels can be potentially transmitted. However, to implement a conventional spatial multiplexing system that accommodates the same number of channels, NM transmitter/receiver aperture pairs and $NM \times NM$ MIMO processing for crosstalk mitigation would be required. Moreover, although the dimensions of MIMO processing are the same, the MIMO processing of the proposed scheme potentially has a lower computation complexity than conventional $NM \times NM$ spatial multiplexing, given that its channel matrix ideally contains N diagonal $M \times M$ sub-matrices. On the other hand, to implement a pure OAM multiplexing system, different NM OAM beams are needed to achieve NM independent data streams. Since the OAM beam diverges approximately as the square root of $|\ell|$ and beams with larger ℓ diverge more, a larger number of OAM beams used for multiplexing may result in larger beam sizes at the receiver such that the recovered power decreases and the BER increases, ultimately limiting system performance.

Although OAM multiplexing and conventional spatial multiplexing have different implementations, they both utilize spatial degrees of freedom for data transmission. A fixed volume that is available for placing transmitter or receiver apertures provides certain spatial degrees of freedom for both multiplexing techniques [48-50]. The simultaneous utilization of both multiplexing techniques explored in this work does not mean that the full benefits of OAM and conventional spatial multiplexing can be reaped at the same time, but rather that the available spatial degrees of freedom might potentially be flexibly distributed between these two multiplexing techniques. For example, if a given volume is divided into a larger number of sub-apertures, more spatial data streams from sub-apertures could be available but clearly each aperture would support fewer OAM channels. Specifically, a fixed volume would limit the number of accommodated apertures and the size of each aperture [50-52]. Moreover, a smaller sized aperture pair implies a more limited Fresnel number of the link, imposes constraints on the spatial bandwidth for multiplexing OAM modes, and indicates that fewer OAM channels can be efficiently transmitted [53]. Therefore, there might exist system design trade-offs when utilizing both techniques, especially as it pertains to approaching the theoretical spatial dimension limit

and thus transmission capacity. This trade-off depends on many factors, including the spatial shape of the volume, the link distance and channel quality (i.e., signal SNR). For a given volume, maximizing the accommodated data channels and system capacity with a particular implementation using the two multiplexing techniques represents an important question. It must be emphasized that OAM and spatial multiplexing have different implementation advantages. OAM allows the easy implementation of analogue separation of modes, which can be important particularly at extremely high data rates. Spatial multiplexing provides greater flexibility for filling irregularly shaped volumes or apertures, including non-contiguous apertures. Thus, for a particular volume, the division of spatial aperture and the use of OAM multiplexing in each or some of the divided apertures may allow more flexibility to fit with the available volume shape and processing capabilities.

When considering the 1.8-meter distance, two OAM modes and two aperture pairs reported in this paper, we believe the proposed approach could potentially be expanded to longer distances and scaled to a larger number of aperture pairs and OAM modes, provided that sufficient power and reasonably low crosstalk for each channel is obtained through careful system design. Specifically, there exists a trade-off between the number of aperture pairs N and the number of OAM beams M in each aperture that can be accommodated, and these numbers are limited by various factors, including system volume, aperture size, and link distance. Given a fixed receiver aperture size, the larger beam size at the receiver for a larger OAM ℓ value may lead to a decrease in recovered power of channel ℓ and an increase in received power of other channels (e.g., inter-modal crosstalk). Such crosstalk might cause a link outage or reduce the rank of channel sub-matrices that results in a decreased channel capacity.

REFERENCES

[1] V. Chandrasekhar, J. G. Andrews, A. Gatherer, "Femtocell networks: A survey," *IEEE Communications Magazine* 46, 59-67 (2008).

[2] D. Halperin, S. Kandula, J. Padhye, P. Bahl, D. Wetherall, "Augmenting data center networks with multi-gigabit wireless links," *Proc. of ACM SIGCOMM Computer Communication Review* 41, 38-49 (2011).

[3] S. Koenig *et al.*, "Wireless sub-THz communication system with high data rate," *Nature Photonics* 7, 977–981 (2013).

[4] P. Driessen, G. Foschini, "On the capacity formula for multiple input-multiple output wireless channels: a geometric interpretation," *IEEE Transactions on Communications* 47, 173-176 (1999).

[5] A. Paulra, D. Gore, R. U. Nabar, H. Bolcksei, "An overview of MIMO communications—A key to Gigabit wireless," *Proceedings of IEEE* 92, 198-218 (2014).

[6] J. H. Winters, "On the capacity of radio communication systems with diversity in a Rayleigh fading environment," *IEEE J. Sel. Areas Commun.* 5, 871–878 (1987).

[7] G. J. Foschini, M. J. Gans, "On limits of wireless communications in a fading environment when using multiple antennas," *Wireless Personal Communications* 6, 311–335 (1998).

[8] A. Paulraj, D. Gore, R. Nabar, *Multiple Antenna Systems*. (Cambridge University Press, Cambridge, U.K., 2003).

[9] A. Hutter, F. Platbrood, J. Ayadi, "Analysis of MIMO capacity gains for indoor propagation channels with LOS component," *IEEE International Symposium on Personal, Indoor and Mobile Radio Communications* 3, 173-176 (2002).

[10] J. S. Jiang, M. A. Ingram, "Spherical wave model for short-range MIMO," *IEEE Transactions on Communications* 53, 1534-1541 (2005).

[11] I. Sarris, A. Nix, "Design and performance assessment of maximum capacity MIMO architectures in line-of sight," *IEE Proc. -Commun*. 153, 482-488 (2006).

[12] F. Bohagen, P. Orten, G. E. Oien, "Design of optimal high-rank line-of-sight MIMO channels," *IEEE Transactions on Wireless Communications* 6, 1420-1425 (2007).

[13] F. Bohagen, P. Orten, G. E. Oien, "On spherical vs. plane wave modeling of line-of-sight MIMO channels," *IEEE Transactions on Communications* 57, 841-849 (2009).

[14] C. Sheldon, M. Seo, E.Torkildson, M. Rodwell, U. Madhow, "Four-channel spatial multiplexing over a millimeter-wave line-of-sight link," *Microwave Symposium Digest, IEEE MTT-S International 2009*, 389-392 (2009).

[15] F. Tamburini *et al.*, "Encoding many channels on the same frequency through radio vorticity: first experimental test," *New J. Phys.*14, 033001 (2012).

[16] G. Gibson *et al.*, "Free-space information transfer using light beams carrying orbital angular momentum," *Optics Express* 12, 5448–5456 (2004).

[17] L. Allen, M. Beijersbergen, R. Spreeuw, J. Woerdman, "Orbital angular-momentum of light and the transformation of Laguerre-Gaussian laser modes," *Phys. Rev. A* 45, 8185–8189 (1992).

[18] B. Thidé *et al.*, "Utilization of photon orbital angular momentum in the low-frequency radio domain," *Phys. Rev. Lett.* 99, 087701 (2007).

[19] G. Molina-Terriza, J. P. Torres, L. Torner, "Twisted photons," *Nature Physics* 3, 305–310 (2007).

[20] A. M. Yao, M. J. Padgett, "Orbital angular momentum: origins, behavior and applications," *Advances in Optics and Photonics* 3, 161–204 (2011).

[21] J. Wang *et al.*, "Terabit free-space data transmission employing orbital angular momentum multiplexing," *Nature Photonics* 6, 488–496 (2012).

[22] N. Bozinovic *et al.*, "Terabit-scale orbital angular momentum mode division multiplexing in fibers," *Science* 340, 1545-1548 (2013).

[23] F. Mahmouli, D. Walker, "4-Gbps uncompressed video transmission over a 60-GHz orbital angular momentum wireless channel," *IEEE Wireless Communications Letters* 2, 223–226 (2013).

[24] Y. Yan *et al.*, "High-capacity milimetre-wave communications with orbital angular momentum multiplexing," *Nat. Commun.* 5, 1–9 (2014).

[25] A. Sibille, C. Oestges, A. Zanella, *MIMO: From Theory to Implementation* (Academic Press, 2009).

[26] J. G. Andrews, C. Wan, R. W. Heath, "Overcoming interference in spatial multiplexing MIMO cellular networks," *IEEE Transactions on Wireless Communications* 14, 95-104 (2007).

[27] G. Caire, S. Shamai, "On the achievable throughput of a multi-antenna Gaussian broadcast channel," *IEEE Transactions on Information Theory* 49, 1691-1706 (2003).

[28] Q. Spence, A. Swindlehurst, M. Haardt, "Zero-forcing methods for downlink spatial multiplexing in multiuser MIMO channels," *IEEE Transactions on Signal Processing* 52, 461-471 (2004).

[29] A. F. Molisch, *Wireless Communications* (Wiley, 2nd ed.,2011).

[30] Y. Ren *et al.*, "Experimental demonstration of 16 Gb/s millimeter-wave communications using MIMO processing of 2 OAM modes on each of two transmitter/receiver antenna apertures," *Proc. of IEEE Global Telecommunications Conference*, paper 1569944271 (IEEE 2014).

[31] A. Honda, Z. Li, L. Zhou, K. Kasai, Y. Ohashi, "Development of wireless communication technologies for future multi-Gigabit data transmission," *Proc. of IEEE Asia-Pacific Microwave Conference*, paper TH1F-4 (IEICE 2014).

[32] Y. Ren, Z.Wang, G. Xie, L. Li, Y. Cao, C. Liu, P. Liao, Y. Yan, N. Ahmed, Z. Zhao, A. Willner, N. Ashrafi, S. Ashrafi, R. D. Linquist, R. Bock, M. Tur, A. F. Molisch, and A. E. Willner, "Free-space optical communications using orbital-angular-momentum multiplexing combined with MIMO-based spatial multiplexing," *Opt. Lett.* 40, 4210-4213 (2015).

[33] G. A. Turnbull, D. A. Robertson, G. M. Smith, L. Allen, M. J. Padgett, "The generation of free-space Laguerre-Gaussian modes at millimetre-wave frequencies by use of a spiral phase plate," *Optics Communications* 127, 183–188 (1996).

[34] M. J. Padgett, J. Arlt, N. Simpson, L. Allen, "An experiment to observe the intensity and phase structure of Laguerre-Gaussian laser modes," *American Journal of Physics* 64, 77–82 (1996).

[35] S.M. Mohammadi *et al.*, "Orbital angular momentum in radio—a system study," *IEEE Trans. Antennas Propag.* 58, 565–572 (2010).

[36] O. Edfors, A. J. Johansson, "Is orbital angular momentum (OAM) based radio communication an unexploited area?," *IEEE Trans. Antennas Propag.* 60, 1126–1131 (2012).

[37] S. Zheng, X. Hui, X. Jin, H. Chi, X. Zhang, "Generation of OAM millimeter waves using traveling-wave circular slot antenna based on ring resonant cavity," *Proc. of IEEE International Conference on Computational Electromagnetics*, paper A03-5 (IEEE 2015).

[38] D. Gesbert, M. Shafi, D. S. Shiu, P. J. Smith, A. Naguib, "From theory to practice: an overview of MIMO space-time coded wireless systems," *IEEE J. Sel. Areas Commun.* 21, 281–302 (2003).

[39] J. Yang, J.-J. Werner, G. A. Dumont, "The multimodulus blind equalization and its generalized algorithms," *IEEE J. Sel. Areas Commun.* 20, 997–1015 (2002).

[40] J.-T. Yuan, K.-D. Tsai, "Analysis of the multimodulus blind equalization algorithm in QAM communication systems," *IEEE Transactions on Communications* 53, 1427-14 31 (2005).

[41] M. Ready, R. Gooch, "Blind equalization on radius directed adaptation," *Proc. of International Conference on Acoustics, Speech, and Signal Processing* 3, 1699 (IEEE 1990).

[42] J. R. Treichler, B. G. Agee, "A new approach to multipath correction of constant modulus signals," *IEEE Transactions on Acoustics, Speech, and Signal Processing* 31, 459-472 (2004).

[43] A. Georgiadis, "Gain, phase imbalance, and phase noise effects on error vector magnitude," *IEEE Transactions on Vehicular Technology* 53, 443-449 (2004).

[44] T. Richte *et al.*, "Transmission of single-channel 16-QAM data signals at terabaud symbol rates," *IEEE Journal of Lightwave Technology* 30, 504–511 (2012).

[45] F. Tamburini*et al.*, "N-tupling the capacity of each polarization state in radio links by using electromagnetic vorticity," arXiv:1307.5569v2 (2013).

[46] F. Tamburini, E. Mari, B. Thide, C. Barbieri, F. Romanato, "Experimental verification of photon angular momentum and vorticity with radio techniques," *Applied Physics Lett.* 99, 204102 (2011).

[47] M. Tamagnone, C. Craeye, J. Perruisseau-Carrier, "Comment on 'Encoding many channels on the same frequency through radio vorticity: first experimental test'," *New J. Phys.*14, 118001 (2012).

[48] T. Svantesson, "On the potential of multimode antenna diversity," *Proc. of IEEE 52nd Veh. Technol. Conf. VTS-Fall* 5, 2368-2372 (IEEE 2000).

[49] T. S. Pollock, T. D. Abhayapala, R. A. Kennedy, "Introducing space into MIMO capacity calculations," *J. Telecommun. Syst.* 24, 415-436 (2003).

[50] T. S. Pollock, T. D. Abhayapala, R. A. Kennedy, "Spatial limits to MIMO capacity in general scattering environments," *Proc. of 7th Int. Symp. on DSP for Commun. Syst.*, 49-54 (IEEE 2003).

[51] J. Jensen, M. A. Wallace, "A review of antennas and propagation for MIMO wireless communications," *IEEE Trans. Antennas Propag.* 52, 810-2824 (2004).

[52] L. Hanlen, M. Fu, "Wireless communication systems with-spatial diversity: A volumetric model," *IEEE Trans. Wireless Commun.* 5, 133-142 (2006).

[53] G. A. Tyler, "Spatial bandwidth considerations for optical communication through a free space propagation link," *Optics Letters* 36, 4650-4652 (2011).